Modeling the Melt Transesterification of Polycarbonate

Jyh-Ping Hsu,[1] Jinn-Jong Wong,[2] Shiojenn Tseng[3]

[1]*Department of Chemical Engineering and Institute of Polymer Science and Engineering, National Taiwan University, Taipei, Taiwan 106*
[2]*Material and Chemical Research Laboratories, Industrial Technology Research Institute, Hsinchu, Taiwan 300*
[3]*Department of Mathematics, Tamkang University, Tamsui, Taipei, Taiwan 25137*

Received 24 June 2005; accepted 26 June 2007
DOI 10.1002/app.27419
Published online 11 January 2008 in Wiley InterScience (www.interscience.wiley.com).

ABSTRACT: A mathematical model of the melt transesterification of polycarbonate in a mechanically agitated reactor system without a distillation column is proposed. Penetration theory is applied to the mass-transfer operation of volatile components in both a transesterification reactor and a polymerization reactor by simplification of the flow pattern. The applicability of the proposed model is examined by the comparison of its predictions with experimental data of the collected condensate of volatile components, the end-group ratio, and the weight fraction distribution of the resulting polymer. The end-group ratios have been determined by carbon-13 nuclear magnetic resonance spectroscopy, and the distribution of weight fractions has been measured by gel permeation chromatography. It is shown that the model's predictions are very consistent with the experimental data. © 2008 Wiley Periodicals, Inc. J Appl Polym Sci 108: 694–704, 2008

Key words: esterification; gel permeation chromatography (GPC); modeling; NMR; polycarbonates

INTRODUCTION

Polycarbonate (PC) is an important engineering thermoplastic material with good mechanical and optical properties for various industrial applications.[1] It can be produced by an interfacial phosgenation process and melt transesterification.[2,3] In recent years, the melt transesterification of PC with the starting materials 4,4′-dihydroxy-diphenyl-2,2-propane (BPA) and diphenyl carbonate (DPC) has become more important because the nonphosgene route for DPC synthesis has reached maturity.[4] However, it still has some disadvantages, such as the ease of coloration and the limited molecular weight of the resulting polymers,[2,3] even through it has been extensively employed in industry. The melt transesterification of PC is a reversible reaction, whose byproduct (phenol) must be removed to shift the chemical equilibrium toward a higher molecular weight. As phenol is removed from the reactor, some DPC is also lost.[5,6] Therefore, the melt transesterification of PC is a complex reaction system that involves interactions of polycondensation and evaporation in a reactor.

A conventional transesterification process typically employs a reactor-column system to separate out the byproduct and prevent volatile monomers from being lost from the reactor. However, evaporative loss of DPC through a distillation column has been observed, even when the column is operated at the optimum reflux ratio,[5,6] indicating that preventing the loss of monomers during the melt process of PC using a distillation column is very difficult. The byproduct should typically be removed as soon as it is formed in reversible condensation. Therefore, a polycondensation system without a distillation column can be used in an interesting approach to the quick removal of the byproduct and may be cost-effective in practical situations.

In this article, a new approach to modeling the melt transesterification of PC is proposed. It involves a polycondensation system without a distillation column. Mechanically agitated reactors are employed to homogeneously mix the reaction mixture and rapidly evaporate phenol from the melt. Therefore, the reactor model incorporates kinetic expressions and mass-transfer equations. The kinetic model has been derived from the reaction mechanism based on the nucleophilic substitution on the carbonyl group.[7] A simplified flow pattern and the penetration theory have been used to determine the mass transfer in the stirring reactor for volatile components.

For verifying this model, the experimental data for characterizing the resulting polymer should be brought out with a reliable method. The end-group ratio is one of the most important features of PC prepared by the melt transesterification method. However, end-group analysis of PC is difficult, although the nuclear magnetic resonance (NMR) technique has been widely used in studying polymers.

Correspondence to: J.-P. Hsu (jphsu@ntu.edu.tw).
Contract grant sponsor: National Science Council (Republic of China, Taiwan).

Ma et al.[8] studied the transesterification of PC with caprolactone segments in ethylene terephthalate–caprolactone copolyester with ^{1}H-NMR and ^{1}H–^{1}H-NMR. Jayakannan and Anilkumar[9] performed composition analysis with ^{1}H-NMR for investigating the ester–carbonate exchange in the reactive blending of PC and cycloaliphatic polyester. Hagenaars et al.[10] described the quantification of the hydroxyl end group with ^{1}H-NMR. However, they did not describe in detail how the end groups were quantified with ^{13}C-NMR. In this article, end-group analysis was performed with ^{13}C-NMR techniques, and the qualification procedure is discussed in detail in a later section.

EXPERIMENTAL

Materials

DPC (>99.5%, mp 5 79.28°C; INBO Chemical Engineering Co., Shanghai, China), BPA (>99.9%; Taiwan Prosperity Chemical Co., Taipei, Taiwan), and 4-dimethylaminopyridine (DAMP; >99.0%; Aldrich, Milwaukee, WI) were used as received.

Reactor system

With reference to Figure 1, melt polycondensation was conducted with a two-stage reaction system. The volume of the transesterification reactor (R-100) was around 70 L, and its diameter was 44.0 cm. It was centrally mounted on a standard marine propeller with four symmetric baffles. The diameter of the impeller was 14.0 cm. The volume of the polymerization reactor (R-200) was around 50 L, and its diameter was 42.4 cm. A helical ribbon-type impeller was centrally mounted on it. The width of the ribbon was 7 cm. Both R-100 and R-200 were stainless steel jacketed reactors heated by heating oil in the jacket. The reactor system was purged with high-purity nitrogen before the starting materials were charged. Then, the catalyst (DAMP) and starting materials (DPC and BPA) with a particular molar ratio were fed into R-100. The phenol vapor was liberated during transesterification under reduced pressure. The vapor was condensed by passage through the condenser (E-100), and the condensate was collected in a collection vessel (V-100) with a sight glass and a calibrated scale for reading the volume.

When the reaction of the transesterification reached a particular temperature and pressure and the volume of the condensate was no longer increasing, the reacting mixture was transferred to R-200 by vapor pressure and gravity. A higher temperature generally corresponded to the need for a stronger vacuum, which was needed to promote

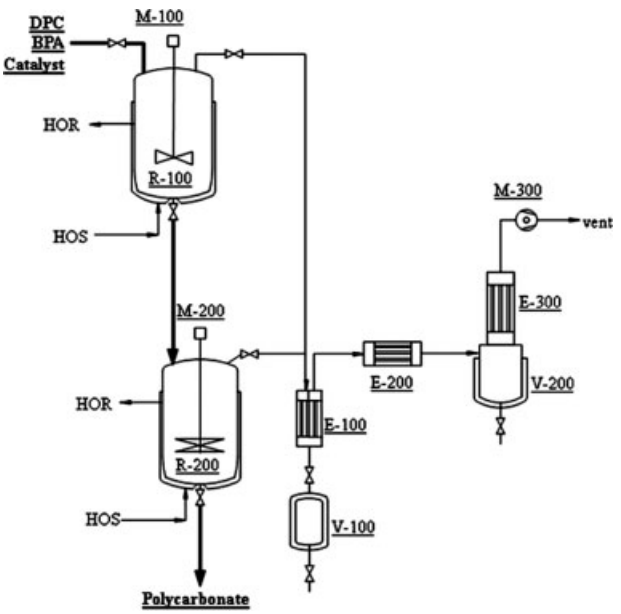

Figure 1 Experimental setup. R-100 and R-200 are the first- and second-stage reactors, respectively; M-100 and M-200 are the agitators of R-100 and R-200, respectively; V-100 and V-200 are the receivers of the condensate; E-100, E-200, and E-300 are the condensers; M-300 is the vacuum pump; HOS is the heating oil supply; and HOR is the heating oil return.

polymerization. The current of the agitator was used to monitor the viscosity of the polymer melt. The agitation was stopped when the current reached the desired value. Finally, the molten polymer was ejected from the reactor under pressure. The polymer melt was cooled to produce thin strings by passage through a water bath. The polymer strings were then palletized.

The molecular weight distributions of the PC samples were measured by gel permeation chromatography (GPC). The GPC system was a Waters LC system equipped with a Waters 610 fluid unit, a Waters 717 Plus automatic sampler, and a Waters 410 differential refractometer with Waters Styragel HR1 and HR2 columns. The dry samples were dissolved in tetrahydrofuran, which was also used as the eluent at a flow rate of 1 mL/min at 20°C. The molecular weight was calibrated with a narrow weight-average molecular weight standard polystyrene and analyzed with Waters Millennium software.

NMR spectra were recorded on a Varian AS500 NMR spectrometer at 125 MHz for ^{13}C-NMR. Deuterated chloroform ($CDCl_3$) was used as the solvent, and tetramethylsilane was used as the internal standard. The PC samples were dissolved in $CDCl_3$ as a 5 wt % solution. Data were acquired and the peaks were integrated with Varian VNMR 6.1 software. The ratio of the amount of the terminal phenolic group to that of the terminal phenyl group was

TABLE I
Structures of the Polymers

Polymer	Structure
A_n	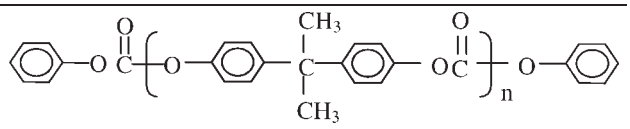
S_n	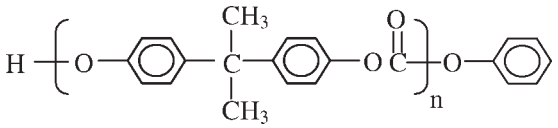
B_n	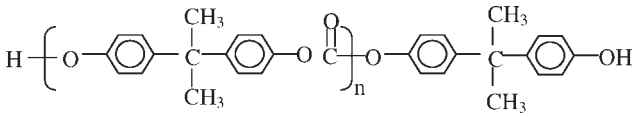

determined from these data. The procedure for data analysis is described in later sections.

REACTOR MODEL

The reactor model is a set of non-steady-state macroscopic mass balance equations that include kinetic rate expressions and evaporation rate equations. The kinetic model of the melt transesterification of DPC and BPA has been proposed in an earlier report by the authors.[7] Under ideal conditions, the system includes only two kinds of terminal end groups. They are either phenolic (—AR—OH) or phenyl (—O—AR) end groups, and this indicates that polymer oligomers fall into three categories: A_n with phenoxy groups at both chain terminals, S_n with phenoxy and phenolic groups at each chain terminal, and B_n with phenolic groups at both chain terminals. Table I presents the structures of A_n, S_n, and B_n, where n is the number of repeating units. When n equals 0, A_0 is DPC and B_0 is BPA. A_n, S_n, and B_n can form different reaction combinations. The overall stoichiometric relationships among reactants and products can be expressed as follows:

$$A_n + S_m \rightleftharpoons A_{n+m} + \text{Phenol} \quad (1)$$

$$A_n + B_m \rightleftharpoons S_{n+m+1} + \text{Phenol} \quad (2)$$

$$S_n + S_m \rightleftharpoons S_{n+m} + \text{Phenol} \quad (3)$$

$$S_n + B_m \rightleftharpoons B_{n+m} + \text{Phenol} \quad (4)$$

The volatile species in the reaction system are assumed to be only the DPC and phenol. The mass balance equations of the reactor are expressed as follows:

$$\frac{dX_0}{dt} = VR_{A_0} - N_D \quad (5)$$

$$\frac{dX_n}{dt} = VR_{A_n} \quad (n \geq 1) \quad (6)$$

$$\frac{dZ_n}{dt} = VR_{B_n} \quad (n \geq 0) \quad (7)$$

$$\frac{dY_n}{dt} = VR_{S_n} \quad (n \geq 1) \quad (8)$$

$$\frac{dP}{dt} = VR_P - N_P \quad (9)$$

where X_n is the amount of A_n in the reaction mixture (mol), Y_n is the amount of S_n in the reaction mixture (mol), Z_n is the amount of B_n in the reaction mixture (mol), and P is the amount of phenol in the reaction mixture (mol). R_{A_0} (mol/L min), R_{A_n} (mol/L min), R_{B_n} (mol/L min), R_{S_n} (mol/L min), and R_p (mol/L min) are the reaction rates of formation of A_0, A_n, B_n, S_n, and phenol, respectively. N_P is the mass-transfer rate of phenol from the liquid phase to the vapor phase (mol/min). N_D is the mass-transfer rate of DPC from the liquid phase to the vapor phase (mol/min). V is the reaction volume (L).

The reaction rates R_{A_0}, R_{A_n}, R_{B_n}, R_{S_n}, and R_p and the mass-transfer rates N_P and N_D must be determined before eqs. (5)–(9) can be solved. Because eqs. (1)–(5) represent an overall stoichiometric relation between reactants and products, they can-

not be used directly to elaborate the reaction mechanisms involved, especially the role of the catalyst. According to the earlier report on the kinetic model of the melt transesterification of DPC and BPA,[7] the melt transesterification of DPC and BPA is of a reversible nature; the forward reaction is second-order in the concentrations of DPC and catalyst, and the reverse reaction is third-order in the concentrations of the phenol, oligomer, and catalyst. The reaction rates of the monomers and the polymeric species can be expressed as follows:

$$R_{A_0} = -\frac{2kCX_0}{V^2} + \frac{k'}{V^3}\left(\sum_{l=1}^{\infty}\frac{(l+1)X_l}{l} + \sum_{l=1}^{\infty}\frac{lY_l}{2l-1}\right)CP \quad (10)$$

$$R_{A_n} = -\frac{2kC}{V^2}\frac{X_n}{n+1} + \frac{kC}{V^2}\left[\sum_{m=0}^{n}\frac{2X_{n-m}}{n-m+1}\frac{Y_m}{\sum Y_i + 2\sum Z_i}\right] - \frac{(n+1)k'}{V^3}CX_nP + \frac{k'}{V^3}\left(\sum_{l=n+1}^{\infty}\frac{(l+1)X_l}{l} + \sum_{l=n+1}^{\infty}\frac{lY_l}{2l-1}\right) \times CP \quad (n \geq 1) \quad (11)$$

$$R_{B_0} = -\frac{kC}{V^2}\left[\sum_{m=0}^{\infty}\frac{2X_m}{m+1} + \sum_{m=1}^{\infty}\frac{Y_m}{m}\right]\left(\frac{2Z_0}{\sum Y_i + 2\sum Z_i}\right) + \frac{k'}{V^3}\left[\sum_{m=1}^{\infty}\frac{mY_m}{2m-1} + \sum_{m=1}^{\infty}Z_m\right]CP \quad (12)$$

$$R_{B_n} = -\frac{kC}{V}\left[\sum_{m=0}^{\infty}\frac{2X_m}{m+1} + \sum_{m=1}^{\infty}\frac{Y_m}{m}\right]\left(\frac{2Z_n}{\sum Y_i + 2\sum Z_i}\right) + \frac{kC}{V}\left(\sum_{m=0}^{n-1}\frac{Y_{n-m}}{n-m}\right)\left(\frac{2Z_m}{\sum Y_i + 2\sum Z_i}\right) - \frac{nk'}{V^2}CZ_nP + \frac{k'}{V^2}\left(\sum_{m=n+1}^{\infty}\frac{mY_m}{2m-1} + \sum_{m=n+1}^{\infty}Z_m\right)CP \quad (n \geq 1) \quad (13)$$

$$R_{S_1} = -\frac{kC}{V}\left[Y_1 + \left(\sum_{m=0}^{\infty}\frac{2X_m}{m+1} + \sum_{m=1}^{\infty}\frac{Y_m}{m}\right)\left(\frac{Y_1}{\sum Y_i + 2\sum Z_i}\right) - 2X_0\frac{2Z_0}{\sum Y_i + 2\sum Z_i}\right] - 2X_0\frac{2Z_0}{\sum Y_i + 2\sum Z_i} - \frac{k'}{V^2}Y_1CP + \frac{k'}{V^2}\left(\sum_{l=1}^{\infty}\frac{(l+1)X_l}{l} + \sum_{l=1}^{\infty}Z_l + \sum_{l=2}^{\infty}\frac{2lY_l}{2l-1}\right)CP \quad (14)$$

$$R_{S_n} = -\frac{kC}{V^2}\frac{Y_n}{n} - \frac{kC}{V^2}\left(\sum_{m=0}^{\infty}\frac{2X_m}{m+1} + \sum_{m=1}^{\infty}\frac{Y_m}{m}\right)\left(\frac{Y_n}{\sum Y_i + 2\sum Z_i}\right) + \frac{2kC}{V}\sum_{m=0}^{n-1}\frac{X_{n-m-1}}{n-m}\frac{2Z_m}{\sum Y_i + 2\sum Z_i} + \frac{kC}{V}\sum_{m=1}^{n-1}\frac{Y_{n-m}}{n-m}\frac{Y_m}{\sum Y_i + 2\sum Z_i} - \frac{nk'}{V^2}Y_nCP + \frac{k'}{V^2}\left(\sum_{l=n}^{\infty}\frac{(l+1)X_l}{l} + \sum_{l=n}^{\infty}Z_l + \sum_{l=n+1}^{\infty}\frac{2lY_l}{2l-1}\right)CP \quad (n \geq 2) \quad (15)$$

$$R_P = \frac{2kC}{V^2}\sum_{m=0}^{\infty}\frac{X_m}{m+1} + \frac{kC}{V^2}\sum_{m=1}^{\infty}\frac{Y_m}{m} - \frac{k'}{V^3} \times \left(\sum_{m=1}^{\infty}(m+1)X_m + \sum_{m=1}^{\infty}mY_m + \sum_{m=1}^{\infty}mZ_m\right)CP \quad (16)$$

where C represents the total quantity of the active catalyst (mol) based on the assumption that the catalyst does not run off during the reaction and that the activity of the catalyst does not change during the reaction. Therefore, the total quantity of the catalyst in the calculation is set to be a constant. k is the forward reaction rate constant (L/mol min), and k' is the reverse reaction rate constant (L^2/mol^2 min). The rate constants used in this work are

$$k = (2.762 \times 10^{11})\exp(-13{,}962(\text{cal/mol})/RT) \quad (17)$$

$$k' = (3.21 \times 10^{10})\exp(-12{,}021(\text{cal/mol})/RT) \quad (18)$$

where R is the gas constant (1.987 cal/mol K) and T is the absolute temperature.

The volatile components, phenol and DPC, evaporate from the liquid phase to the vapor phase during the reaction. It has been assumed that the mass-transfer resistance in the gas film is negligible. The mass-transfer rate across the vapor–liquid interface can generally be expressed as follows:

$$N_j = kl_j a(C_j - C_j^*)/1000 \quad (19)$$

where suffix j refers to P (phenol) or D (DPC), kl_j is the overall mass-transfer coefficient (cm/min) of component j, a is the interfacial mass-transfer area (cm^2), C_j is the concentration of volatile component j in the liquid phase (mol/L), and C_j^* is the equilibrium concentration of volatile component j at the liquid–vapor interface (mol/L).

In melt transesterification, the liquid film is assumed to be very thick at the liquid–vapor interface. With the idealized penetration theory,[11] the overall mass-transfer coefficient is

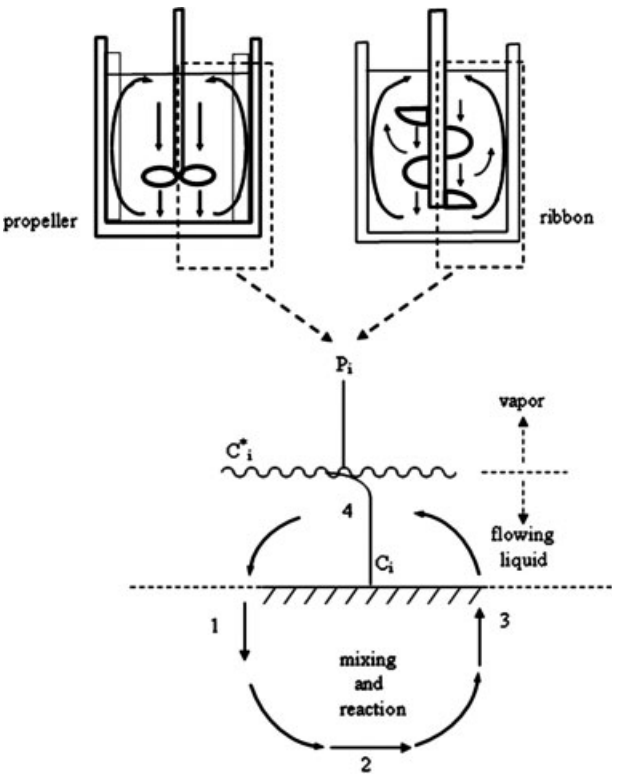

Figure 2 Simplified flow pattern in the reactors.

$$kl_j = 2\sqrt{\frac{D_j}{\pi t_e}} \tag{20}$$

where D_j is the diffusivity of component j in the reaction mixture (cm^2/min) and t_e is the exposure time. D_P is assumed to be

$$D_j = D_{0j}\exp(-E_{Dj}/RT) \tag{21}$$

where suffix j indicates P (phenol) or D (DPC) and D_{0j} and E_{Dj} are adjustable parameters. In this study, D_{0P} is 1.22×10^{17} (cm^2/min), E_{Dp} is 38,700 (cal/mol), D_{0D} is 1.31×10^{16} (cm^2/min), and E_{DD} is 42,400 (cal/mol).

t_e (min) is the period for which the fluid is exposed at the vapor–liquid interface and depends on the type of impeller and the rotation speed of the agitator. In Figure 2, the axial flow impeller, such as that which comprises the propeller and ribbon, perpendicularly moves the fluid. The fluid moves around in the reactor and rises to the vapor–liquid interface before flowing down into the reaction mixture. The real flow pattern in an agitated reactor may be very complicated. The model presented in Figure 2(A,B) has been further simplified as presented in Figure 2(C). When the process begins and agitation induces the circulation flow of the reaction mass, it is assumed to begin at position 1, pass through position 2, and arrive at position 3. Reactions and mixing occur as the reaction mass flows along path 1-2-3. t_e is determined for the reaction mass exposed to the vapor–liquid interface as it travels path 3-4-1. At this time, the volatile components can escape from the liquid phase into the vapor phase. The flow rate produced by the agitator can be expressed as follows:[12]

$$Q = N_Q N_R D_A^3/1000 \tag{22}$$

where Q denotes the pumping rate produced by the agitator (L/min), N_Q is the pump number (for a marine propeller, N_Q is 0.5, and for a helical ribbon impeller, N_Q is 0.1), N_R is the rate of rotation of the agitator (min^{-1}), and D_A is the characteristic diameter of the stirring component (cm). t_e is determined as follows:

$$t_e = \frac{\pi r^3}{2000Q} \tag{23}$$

where r is the radius of the reactor. Mass-transfer area a is the free exposed surface of the reactor and can be expressed as follows:

$$a = \pi r^2 \tag{24}$$

For the nonvolatile components, no concentration gradient is assumed between the bulk liquid phase and the liquid film at the liquid–vapor interface. In eq. (19), the interfacial concentration of the volatile species is

$$C_j^* = \frac{C_t - \sum C_j}{1 - \sum x_j^*} x_j^* \quad (j = D, P) \tag{25}$$

C_t, C_D, and C_P are

$$C_t = \frac{\sum X_i + \sum Y_i + \sum Z_i + P}{V}, C_D = \frac{X_0}{V}, C_P = \frac{P}{V} \tag{26}$$

The vapor phase is assumed to follow the ideal gas law; the molar fraction of DPC and phenol at the interface can thus be expressed as

$$x_D^* = \frac{P_t y_D}{\gamma_D P_D^0} \tag{27}$$

$$x_P^* = \frac{P_t y_P}{\gamma_P P_P^0} \tag{28}$$

where P_t is the total pressure (mmHg); P_D^0 and P_P^0 are the saturated vapor pressures of DPC and phenol (mmHg), respectively; and γ_D and γ_P are the activity coefficients of DPC and phenol, respectively.

The thermodynamic properties, P_D^0 and P_P^0, can be expressed as follows:[6,13]

$$\log P_D^0 = \left(-\frac{14.76 \times 10^3}{1.987}\right)\frac{1}{T} + 19.5521 \quad (29)$$

$$\log P_P^0 = 7.13457 - \frac{1516.072}{T - 98.581} \quad (30)$$

The activity of phenol and DPC can be expressed as follows:

$$\gamma_j = \left(\frac{1}{m_j}\right)\exp\left(1 - \frac{1}{m} + \chi_j\right), \quad (j = D, P) \quad (31)$$

where γ_j is the activity coefficient of component j, χ_j is the Flory–Huggins interaction parameter, and m_j is the ratio of the molar volume of the polymer to the molar volume of component j. For component j in the polymer system, χ_j is expressed as follows:[13]

$$\chi_j = 0.34 + \frac{\hat{v}}{RT}(\delta_j - \delta_{\text{ploy}})^2 \quad (32)$$

where δ_j is the solubility parameter of component j ($\text{cal}^{1/2}/\text{cm}^{3/2}$) and δ_{poly} is the solubility parameter of the polymer ($\text{cal}^{1/2}/\text{cm}^{3/2}$). For a semibatch reactor, the temporary volume can be expressed as

$$V = V_0 - \hat{v}_P M_P - \hat{v}_{\text{DPV}} M_D \quad (33)$$

where V_0 is the volume of the initial charge (L) and $\hat{v}_P$ and $\hat{v}_{\text{DPC}}$ are the molar volumes of phenol and DPC (L/mol), respectively. Phenol is continuously removed outside the reactor; the accumulated amount of phenol is M_P (mol), and the accumulated amount of DPC is M_D (mol):

$$M_P = \int_0^t N_P dt \quad (34)$$

$$M_D = \int_0^t N_D dt \quad (35)$$

The initially charged reactants are DPC and BPA, so the initial volume is

$$V_0 = \hat{v}_{\text{DPC}}\text{DPC}_0 + \hat{v}_{\text{BPA}}\text{BPA}_0 \quad (36)$$

where $\hat{v}_{\text{DPC}}$ and $\hat{v}_{\text{BPA}}$ are the molar volumes of DPC and BPA, respectively, and DPC_0 and BPA_0 are the initial amounts of DPC and BPA (mol), respectively.

RESULTS AND DISCUSSION

PC samples MTPC1, MTPC2, and MTPC3 were prepared at the reactor temperature and pressure shown in Figure 3. The DPC/BPA molar ratios in the feed were 1.03, 1.10, and 1.05, respectively. The concentrations of the catalyst were 200, 100, and 5 ppm based on the initial concentration of BPA in each test. The process time began when all of the materials were fed into the transesterification reactor. The reactor temperature was gradually elevated to keep the reacting mixture in a molten state, and the reactor pressure was reduced at a particular rate in each case. The pressure profile of MTPC1 declined sharply, but in MTPC2 and MTPC3, the decline was more gradual. The stirring rates were each kept constant at 150 and 60 rpm in the transesterification reactor and the polymerization reactor, respectively. Clearly, a wide operating window was established to examine the applicability of the proposed model. The governing equations, eqs. (5)–(9), were solved numerically with the DIVPRK subroutine of Microsoft Fortran PowerStation. The operating conditions were applied as inputs to determine the amount of the condensate, the end-group ratio, and the weight fraction distribution in the resulting polymers.

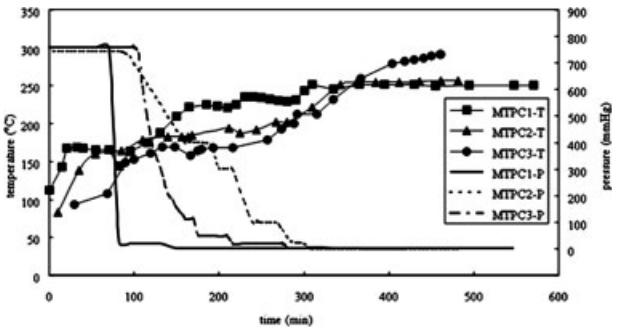

Figure 3 Temperature and pressure profiles for the preparation of PC samples MTPC1, MTPC2, and MTPC3. The DPC/BPA monomer ratios were 1.02 for MTPC1, 1.10 for MTPC2, and 1.05 for MTPC3. The concentrations of the catalyst used for MTPC1, MTPC2, and MTPC3 were 200, 100, and 5 ppm, respectively. The reactor temperatures are designated (■) MTPC1-T, (▲) MTPC2-T, and (●) MTPC3-T. The reactor pressures are designated (—) MTPC1-P, (- - -) MTPC2-P, and (- · - · -) MTPC3-P.

Under the aforementioned operating conditions, the specific mass-transfer coefficient in the case of MTPC3 was 0–3 (1/min) for phenol and 0–0.3 (1/min) for DPC, as shown in Figure 4. The specific mass-transfer coefficients in the other two cases were similar to that for MTPC3 and are not shown here. This figure indicates that the specific mass-transfer coefficient increased with the reactor temperature. The curves were interrupted around 200°C because the reactant was transferred from the transesterification reactor to the polymerization reactor. The impeller was changed to the helical ribbon type, and the stirring speed was reduced, so the specific mass-transfer coefficient again increased with the reactor temperature. According to eqs. (20)–(23), the temper-

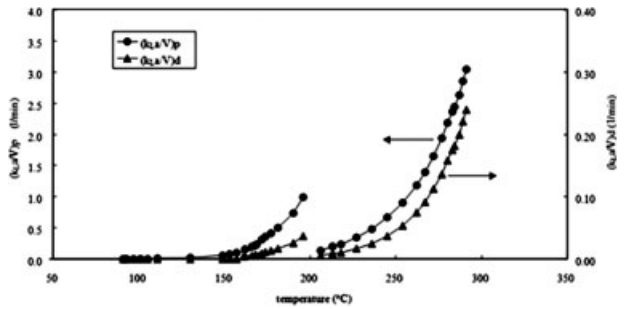

Figure 4 Specific mass-transfer coefficients of (●) phenol $[(k_La/V)_p]$ and (▲) DPC $[(k_La/V)_d]$ for MTPC3. The solid lines are guides for the eye.

ature, type of impeller, and stirring speed affected the specific mass-transfer coefficient. However, the effect of the melt viscosity on the mass-transfer coefficient is not considered herein.

The amount of the condensate of the volatile components collected at the reactor outlet is one of the important measurable physical quantities. In the model, it is the sum of M_D and M_P, as expressed in eqs. (35) and (36). Phenol is mixed with DPC as a result of the chemical reaction and evaporative loss of the monomer. Stoichiometrically, the ultimate amount of phenol produced in melt transesterification is double the amount of BPA fed if all of the hydroxyl groups of BPA are consumed in the reaction. The ratio of the amount of the collected condensate to the ultimate amount of phenol, as shown in Figure 5, was determined in each case (MTPC1, MTPC2, and MTPC3) under each condition. The model outputs closely agree with the measured data. Of course, the contribution of evaporative loss can be determined from eq. (36) alone. The estimated DPC losses were 5, 6, and 7% for MTPC1, MTPC2, and MTPC3, respectively. Even though the composition of the collected condensate was not traced experimentally in this study, further end-group analysis can provide additional information, as described next.

The most important task of modeling a polymerization process is to predict the properties of the final polymer under given process conditions. The population of each species throughout the reaction must be accurately monitored. Essentially, this model can be applied to extract the concentrations of A_n, B_n, and S_n in the system. Initially, the system included only DPC (A_0) and BPA (S_0). The number of phenyl end groups (—phenyl) was equal to $2A_0$, and the number of phenolic end groups (—ArOH) was equal to $2S_0$. Various oligomers or short-chain polymers were generated, accumulated, and then consumed in the reaction. Therefore, the number of terminal phenolic end groups and the number of terminal phenoxy end groups dynamically shifted to $\sum(2A_n + B_n)$ and $\sum(2S_n + B_n)$. The end-group ratio [—ArOH]/[—phenyl] (where [—ArOH] is the phenolic end-group concentration and [—phenyl] is the phenyl end-group concentration), as shown in Figure 6, was calculated as $\sum(2A_n + B_n)/\sum(2S_n + B_n)$. In the case of MTPC1, the curve rises gradually and stays in an equilibrium state. In the case of MTPC2, the end-group ratio profile varies drastically toward the end of polymerization. However, in the MTPC3 case, the end-group ratio profile evolved gradually during the reaction.

The end-group ratio analysis for PC samples was determined by ^{13}C-NMR. Assignments and chemical shifts of ^{13}C-NMR of the reaction components and PC chain structure are summarized in Table II. All samples expectably showed strong characteristics of the PC chain structure.[14] The chemical shifts at 30.9 (C1: methyl carbon), 42.6 (C2: quaternary carbon), 120.3 and 127.9 (C4 and C5: unsubstituted aromatic carbon), 148.3 and 149.1 (C3 and C6: substituted aromatic carbon), and 152.1 ppm (C7: carbonate group) characterize the PC chain structure. Note that some small peaks can be observed wildly spread around

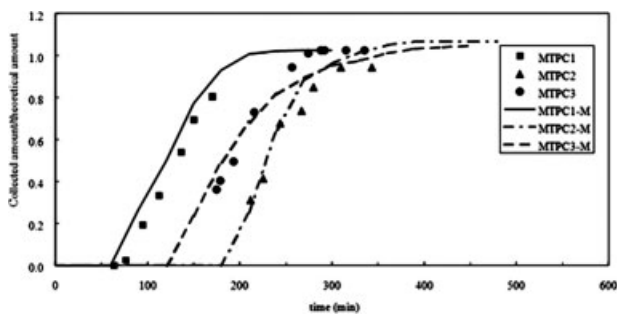

Figure 5 Ratio of the condensate in the preparation of PC samples MTPC1, MTPC2, and MTPC3. The discrete symbols represent the experimental data; the curves plot the values on the basis of the proposed model. The experimental data are for (■) MTPC1, (▲) MTPC2, and (●;) MTPC3. The modeling results are designated (—) model MTPC1, (- · - · -) model MTPC2, and (- - -) model MTPC3.

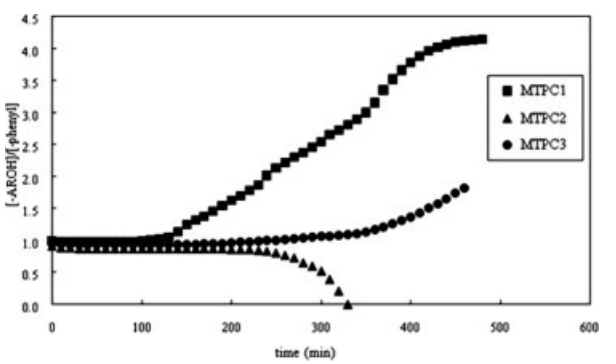

Figure 6 Temporal variation of the end-group ratio determined by the proposed model for (■) MTPC1, (▲) MTPC2, and (●) MTPC3.

TABLE II
Assignments and Chemical Shifts of Liquid-Phase ^{13}C-NMR of the PC Chain Structure

Model compound	Structure	Assignment	Chemical shift						
			Phenol	BPA	DPC	PC[14(b)]	MTPC1	MTPC2	MTPC3
PC	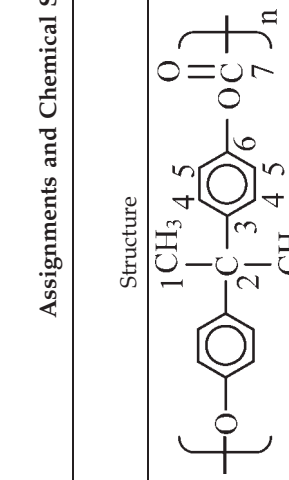	C1		31.0		30.9	30.9	30.8	30.9
		C2		41.3		42.6	42.5	42.5	42.5
		C3				148.3	148.2	148.2	148.2
		C4				127.9	127.8	127.8	127.8
		C5				120.3	120.2	120.2	120.3
		C6				149.1	149.0	148.9	148.9
		C7			151.9	152.1	152.1	152.0	152.0
Phenyl end group		C3′			150.9			151.0	151.0
		C4′	129.8		129.4			129.5	129.5
		C5′	121.1		120.8			120.8	120.8
		C6′			126.1			126.0	126.2
Phenolic end group		C3″		142.5			142.0		142.1
		C4″		127.7		127.9	127.8	127.8	127.8
		C5″	115.6	114.9			114.7		114.7
		C6″	155.0	153.8			153.8		153.8

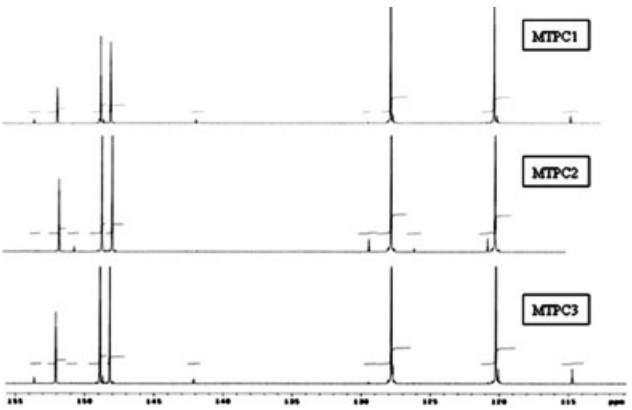

Figure 7 ^{13}C-NMR (125 MHz) spectra of MTPC1, MTPC2, and MTPC3.

115–154 ppm, as shown in Figure 7. In contrast to the chemical shifts of phenol, DPC, and BPA, these chemical shifts appearing at 120.8 (C5′), 126.2 (C6′), 129.5 (C4′), and 151.0 ppm (C3′) can be assigned to the phenyl group, and those appearing at 114.7 (C5″), 127.8 (C4″), 142.1 (C3″), and 153.8 ppm (C6″) can be assigned to the phenolic group.

The NMR signal obtained is directly proportional to the number of nuclei resonating. The ratio of [—ArOH] to [—phenyl] can be calculated from the integration of the absorbance at specific chemical shifts. Accordingly, the ratio of [—ArOH] to [—phenyl] can be expressed as follows:

$$\frac{[-\mathrm{ArOH}]}{[-\mathrm{phenyl}]} = \frac{[\mathrm{C}_6'']}{[\mathrm{C}_3']} = \frac{I_{153.8}}{I_{151.0}} \tag{37.1}$$

$$\frac{[-\mathrm{ArOH}]}{[-\mathrm{phenyl}]} = \frac{[\mathrm{C}_5'']}{[\mathrm{C}_4']} = \frac{I_{114.7}}{I_{129.5}} \tag{37.2}$$

$$\frac{[-\mathrm{ArOH}]}{[-\mathrm{phenyl}]} = \frac{2[\mathrm{C}_6'']}{[\mathrm{C}_4']} = \frac{2I_{153.8}}{I_{129.5}} \tag{37.3}$$

$$\frac{[-\mathrm{ArOH}]}{[-\mathrm{phenyl}]} = \frac{[\mathrm{C}_5'']}{2[\mathrm{C}_3']} = \frac{I_{114.7}}{2I_{151.0}} \tag{37.4}$$

where I_δ is the integration of the signal occurring at chemical shift δ (ppm). Equations (37.1)–(37.4) show the end-group ratio in different combinations. To minimize noise, the mean value is used as the ratio of [—ArOH] to [—phenyl]. End-group ratio calculations using eqs. (37.1)–(37.4) from ^{13}C-NMR measurements are summarized in Table III. The obtained mean values were 4.33, 0.03, and 1.56 for MTPC1, MPTC2, and MTPC3, respectively. The [—ArOH]/[—phenyl] ratios of the resulting polymers predicted by the model were 4.44, 0, and 1.34 for MTPC1, MPTC2, and MTPC3, respectively. Notice that the three results were obtained with three initial

TABLE III
Calculation of the End-Group Ratio from ^{13}C-NMR

	Integration of the chemical shift (%)				Calculation result				
	151.0	129.5	114.7	153.8	Eq. (37.1)	Eq. (37.2)	Eq. (37.3)	Eq. (37.4)	Mean value
MTPC1	0.00	0.39	1.78	0.80	—	4.56	4.10	—	4.33
MTPC2	0.71	1.97	0.00	0.05	0.070	0.00	0.05	0.00	0.03
MTPC3	0.19	0.63	1.06	0.21	1.105	1.68	0.67	2.79	1.56

ratios (0.98, 090, and 0.952) that were quite close to one another. This implies that a small deviation can lead to a very large departure in the polymer. It is critical in polymer property control. Therefore, a predictable profile of the end-group ratio might be helpful in obtaining a polymer product with desired properties.

The concentrations of A_n, B_n, and S_n in the model can be determined. The weight fraction distributions of samples MTPC1, MTPC2, and MTPC3 are easily determined. Figure 8 compares the predictions with the GPC measurements. The weight fraction distribution predicted by this model is narrower than that obtained by GPC measurement. The GPC profile corresponded to a higher fraction with a chain length of around 80–90, probably resulting from the Kolbe–Schmitt reaction at a high temperature.[3,10]

The PC product has been mentioned previously to comprise A_n, B_n, and S_n, whose microscopic distributions importantly affect product usage. Figure 9 shows the weight fraction distribution of A_n, B_n, and S_n in each case. In the MTPC1 case, in which DPC/BPA was 1.02, the dominant species in the resulting polymer were S_n-type PCs. However, in the MTPC2 case, in which DPC/BPA was 1.10, the dominant species were A_n-type PCs. As expected, in the MTPC3 case, in which DPC/BPA was 1.05, B_n-type PCs dominated the final products. Therefore, the dif-

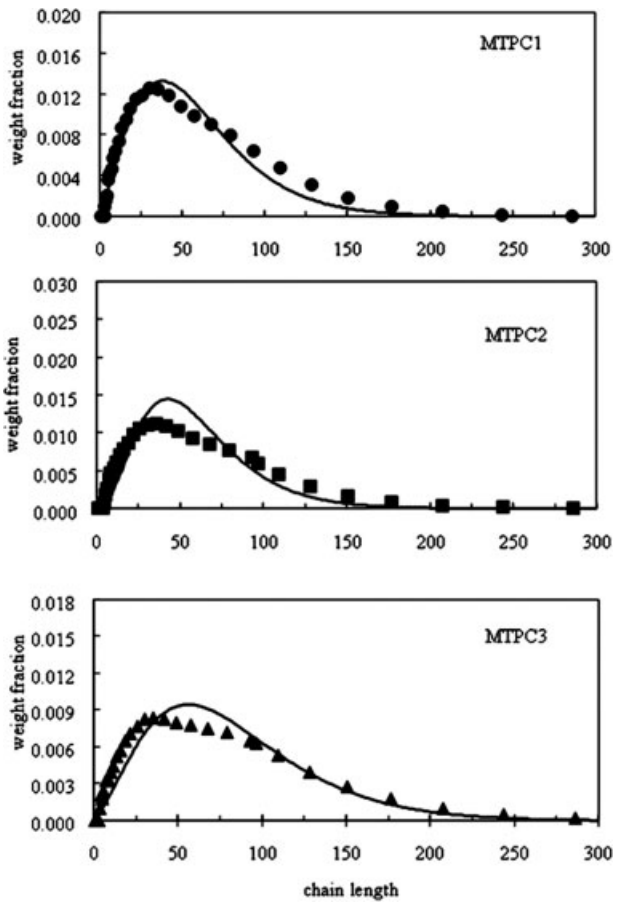

Figure 8 Weight fraction distributions of MTPC1, MTPC2, and MTPC3. The discrete symbols represent the GPC measurements, and the curves are the profiles obtained with the proposed model.

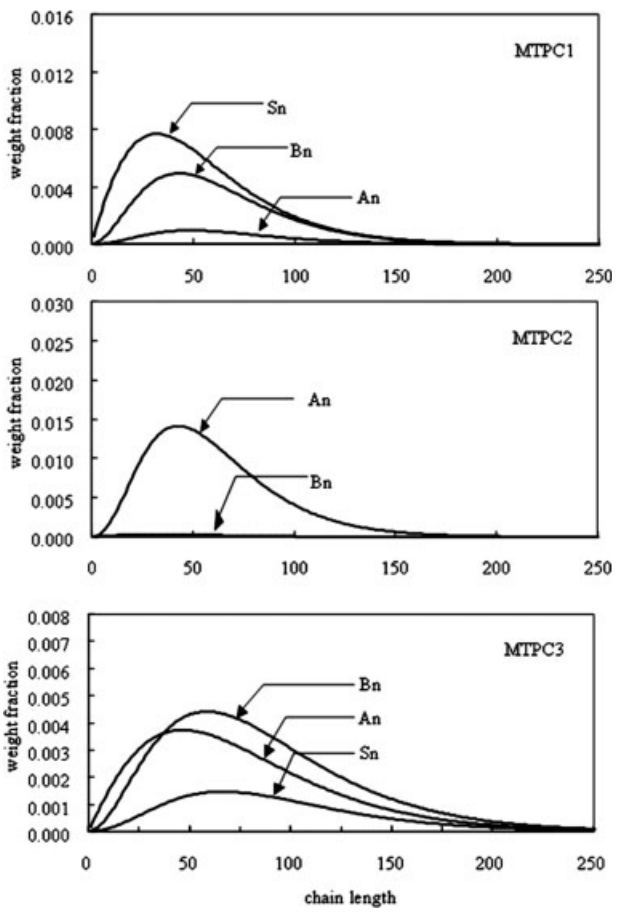

Figure 9 Weight fraction distribution profiles of various PCs in samples MTPC1, MTPC2, and MTPC3 (for the meaning of symbols A_n, B_n, and S_n, see Table I).

ferences in DPC vaporization have a signification effect on the species distribution. The PC products were microscopically observed to differ greatly.

CONCLUSIONS

A mathematical model of the melt transesterification process of PC in a two-stage polycondensation system was developed. Both reactors were mechanically agitated, but different impellers were installed. A simplified flow pattern was applied to interpret the agitation flow of the reacting mass. The proposed model can be used to elucidate the fluid flow, the chemical reaction, and the evaporation that simultaneously occurred within the reactors.

The applicability of this model was examined by a comparison of theoretical predictions with the experimental data under broad operation conditions. The theoretical prediction of the amount of the condensate of the volatile components closely agreed with the amount of condensate collected at the reactor outlet. The DPC losses were 5, 6, and 7% in the MTPC1, MTPC2, and MTPC3 cases, respectively, indicating that the process was satisfactory even though no distillation column was joined to the reactor. Modeling studies revealed that this model could be used to calculate the temporal variation of the end groups throughout the reaction, and the NMR measurements corroborated the predicted end-group ratios of the resulting polymers. A comparison of the weight fraction distributions revealed that the predicted profile was consistent with the GPC measurements.

NOMENCLATURE

[—ArOH]	phenolic end-group concentration
[—phenyl]	phenyl end-group concentration
a	interfacial mass-transfer area (cm^2)
BPA	4,4′-dihydroxy-diphenyl-2,2-propane
BPA_0	amount of 4,4′-dihydroxy-diphenyl-2,2-propane initially charged to the reactor (mol)
C	concentration of the catalyst (mol/L)
$CDCl_3$	deuterated chloroform
C_j	concentration of component j in the liquid phase (mol/L)
C_j^*	equilibrium concentration of component j at the liquid–vapor interface (mol/L)
C_t	concentration of component j in the liquid phase (mol/L)
D_{0j}	adjustable parameter defined in eq. (21)
D_A	characteristic diameter of the stirrer (cm)
DAMP	dimethylaminopyridine
D_j	diffusivity of component j in the reaction mixture (cm^2/min)
DPC	diphenyl carbonate
DPC_0	amount of diphenyl carbonate initially charged to the reactor (mol)
E_{Dj}	adjustable parameter defined in eq. (21)
GPC	gel permeation chromatography
I_δ	integration of the signal occurring at chemical shift δ (ppm)
k	forward reaction rate constant (L/mol min)
k'	reverse reaction rate constant (L^2/mol^2 min)
kl_j	overall mass-transfer coefficient of component j (cm/min)
M_D	accumulated amount of diphenyl carbonate (mol)
M_P	accumulated amount of phenol (mol)
m_j	ratio of the molar volume of the polymer to the molar volume of component j
NMR	nuclear magnetic resonance
N_D	mass-transfer rate of diphenyl carbonate from the liquid phase to the vapor phase (mol/min)
N_P	mass-transfer rate of phenol from the liquid phase to the vapor phase (mol/min)
N_Q	pumping number
N_R	rate of rotation of the agitator (min^{-1})
P	amount of phenol in the reaction mixture (mol)
PC	polycarbonate
P_D^0	saturated vapor pressure of diphenyl carbonate (mmHg)
P_P^0	saturated vapor pressure of phenol (mmHg)
P_t	total pressure (mmHg)
Q	pumping rate produced by the agitator (L/min)
r	radius of the reactor (cm)
R	gas constant (1.987 cal/mol K)
R_{A_0}	reaction rate of A_0 (mol/L min)
R_{A_n}	reaction rate of A_n (mol/L min)
R_{B_n}	reaction rate of B_n (mol/L min)
R_{S_n}	reaction rate of S_n (mol/L min)
R_p	reaction rate of phenol (mol/L min)
T	absolute temperature
t_e	exposure time (min)
V	reaction volume (L)
V_0	initial volume (L)
X_n	amount of A_n in the reaction mixture (mol)
Y_n	amount of S_n in the reaction mixture (mol)
Z_n	amount of B_n in the reaction mixture (mol)
γ_D	activity coefficient of diphenyl carbonate
γ_j	activity coefficient of component j

γ_P activity coefficient of phenol
δ_j solubility parameter of component j ($cal^{1/2}/cm^{3/2}$)
δ_{poly} solubility parameter of the polymer ($cal^{1/2}/cm^{3/2}$)
$\hat{v}_P$ molar volume of phenol (L/mol)
$\hat{v}_{DPC}$ molar volume of diphenyl carbonate (L/mol)
χ_j Flory–Huggins interaction parameter of component j

References

1. Serini, V. Polycarbonates. In Ullmann's Encyclopedia of Industrial Chemistry, 5th ed.; Elvers, B.; Hawkins, S.; Schulz, G., Eds.; VCH: New York, 1992; Vol. A21, p 207.
2. King, J. A., Jr. In Handbook of Polycarbonate Science and Technology; LeGrand, D. G.; Bendler, J. T., Eds.; Marcel Dekker: New York, 2000; p 7.
3. Schnell, H. Chemistry and Physics of Polycarbonates; Polymer Reviews 9; Interscience: New York, 1964; Chapter III.
4. Kim, W. B.; Joshi, U. A.; Lee, J. S. Ind Eng Chem Res 2004, 43, 1897.
5. Woo, B. G.; Choi, K. Y.; Song, K. H.; Lee, S. H. J Appl Polym Sci 2001, 81, 1253.
6. Kim, Y.; Choi, K. Y. J Appl Polym Sci 1993, 49, 747.
7. Hsu, J. P.; Wong, J. J. Polymer 2003, 44, 5851.
8. Zhang, Z.; Luo, X.; Lu, Y.; Ma, D. Eur Polym J 2001, 37, 99.
9. Jayakannan, M.; Anilkumar, P. J Polym Sci Part A: Polym Chem 2004, 42, 3996.
10. Hagenarrs, A. C.; Pesce, J. J.; Bailly, C.; Wolf, B. A. Polymer 2001, 42, 7653.
11. Cussler, E. L. Diffusion, Mass Transfer in Fluid System, 2nd ed.; Cambridge University Press: New York, 1997; Chapter 13.
12. Trambouze, P.; Candeghem, H. V.; Wauquier, J. P. Chemical Reactors, Design/Engineering/Operation; Marshall, N., Translator; Institute Francais du Petrole: Paris, 1988; p 539.
13. Kim, D. H.; Ha, K. S.; Rhee, H. K.; Song, K. H. J Appl Polym Sci 2003, 88, 1010.
14. (a) Sadtler Carbon-13 NMR of Monomer and Polymer Index; Sadtler Research Laboratories: Philadelphia, 1985; Vols. 1–4, D87C; (b) Sadtler Carbon-13 NMR of Monomer and Polymer Index; Sadtler Research Laboratories: Philadelphia, 1985; Vols. 1–4, D115C; (c) Sadtler Carbon-13 NMR of Monomer and Polymer Index; Sadtler Research Laboratories: Philadelphia, 1985; Vols. 1–4, D690C.